On the significance of the climate-dataset recording interval in characterising wind-driven rain and simultaneous wind pressure. Part II: Directional analysis

José M. Pérez-Bella[a], Javier Domínguez-Hernández[a,*], Enrique Cano-Suñén[a], Juan J. del Coz-Díaz[b], Felipe P. Álvarez Rabanal[b]

[a] *Department of Construction Engineering, Engineering and Architecture School, University of Zaragoza, María de Luna, s/n, 50018 Zaragoza, Spain.*

[b] *Department of Construction Engineering, University of Oviedo, Edificio Departamental Viesques nº 7, 33204 Gijón, Spain.*

Abstract

Both semi-empirical methods and CFD simulations use real climate datasets as a basis for determining the building facade exposure to wind-driven rain and simultaneous wind pressure. The time resolution of these datasets and the number of variables considered (commonly rainfall intensity, wind velocity and wind direction) determine the required calculation effort and the accuracy of the result. Omitting the wind direction, a former article (Part I of this research) has analysed the effect of this time resolution on two scalar exposure indices obtained by semi-empirical methods: driving-rain index (aDRI) and driving-rain wind pressure (DRWP). However, the wind direction during precipitation events also causes significant exposure variations between possible facade orientations. Thus, it is also necessary to clarify the influence of the recording interval of the dataset, on the accuracy of the directional semi-empirical calculation of aDRI and DRWP. To meet this challenge, the article examines 10-min, hourly, daily, monthly and annual climate records collected between 2001 and 2016 at 6 Spanish locations, analysing the accuracy of the directional exposure indices associated with each time resolution. The results show that a daily dataset would allow identifying the most exposed orientation with an error less than 45º. However, even the hourly datasets cause errors close to 10% in the exposure values identified on each facade orientation. Finally, adjustment relationships that allow estimating the maximum value of directional exposure from simple scalar indices are obtained.

Keywords

Wind-driven rain; Wind pressure; Building façades; Climatic data; Error

[*] Corresponding author. Department of Construction Engineering, University of Zaragoza (UZ), María de Luna, s/n, 50018, Zaragoza, Spain. Tel.Fax: +34 976 76 21 00.
E-mail address: javdom@unizar.es (Javier Domínguez-Hernández)

1. Introduction

The exposure of buildings to wind-driven rain (WDR) and the simultaneous action of driving-rain wind-pressure (DRWP), allows rainwater to impinge facades, to overcome the surface tension and capillary pressure of the water contained in pores and deficiencies, and finally to penetrate through construction materials [1-2]. This penetration affects the thermal insulation, durability and habitability of the building, causing relevant economic and environmental impacts [3-12].

In the first part of this investigation (Part I), the scalar exposure values of WDR and DRWP exposure in several Spanish sites have been determined by semi-empirical methods [13]. The errors associated with datasets of different time resolutions (i.e., hourly, daily, monthly and annual datasets) have been compared taking 10-min records of rainfall intensity and wind velocity compiled under free-field conditions are the reference. In general, the DRWP exposure value presented greater sensitivity to the recording interval, with significant errors even when using daily datasets. Likewise, the high uncertainty presented by scalar results of WDR exposures calculated based on monthly and annual records were quantified.

In any case, the existence of prevailing wind directions during precipitation events causes important exposure variations between the different facades of the same building. Characterising the WDR and DRWP values in the most exposed facades is therefore a key task in establishing the actual watertightness requirements necessary for the design of the building's enclosures [2, 14-18].

To obtain this directional distribution using semi-empirical methods, a cosine projection is usually added to the scalar equations, thus incorporating the relationship between the wind direction recorded during each precipitation interval and the analysed facade orientation [19-21]. Several studies have already applied this cosine projection method, characterising the directional value of exposure in different regions [22-27]. However, there has been no uniformity in the recording interval of the climatic data used, nor has there been a comprehensive investigation to determine the uncertainty associated with each time resolution of the dataset. As a result, the actual accuracy of the directional exposure values that have been obtained so far by semi-empirical calculations and varied recording intervals is unknown.

This manuscript addresses this lack of information, defining 2 analysis criteria for each time resolution of the dataset: the accuracy of semi-empirical directional results of WDR and DRWP exposures and the correct identification of the orientations subject to exposure. To do so, the study is based on exhaustive climate data collected during 15 years in 6 weather stations located in northwestern Spain characterised by diverse environmental and exposure conditions. The directional calculation is performed considering 24 possible facade orientations (i.e., 15 ° intervals) by applying the cosine projection method and assessing 10-min, hourly, daily, monthly, and yearly climate datasets. Finally, the hypothesis suggested by a previous study to approximate the maximum value of directional exposure from the scalar exposure value identified at the site was examined [27].

Together, both parts of this paper provide valuable guidelines for reinterpreting and contextualising the WDR and DRWP results published so far in the specialised literature. In turn, general adjustments are provided to increase the accuracy of any semi-empirical result (scalar or directional) obtained from climate datasets with low temporal resolution. In addition, they include for the first time an approach to the analysis of these aspects in the DRWP exposure, completing a comprehensive review of the two most relevant climatic factors involved in the penetration of water into building facades.

2. Background

Precipitation events usually occur under recurring climatic conditions, which determine the exposure of buildings to WDR and DRWP and thereby the risk of atmospheric water penetration into their facades. The scalar value of WDR and DRWP exposure only provides general information about the exposure level due to the typical climatic conditions at each location. However, precipitation events are also characterised by prevailing wind directions, which can cause significant differences in exposure between facades of the same building [28-31]. Thus, facades facing these prevailing winds can receive WDR and DRWP exposures close to the scalar value identified at the site, whereas those located leeward can be scarcely affected [22-27].

As for scalar values, the directional distribution of both exposures can be determined by experimental measurements collected "in situ", CFD simulations of wind flow and raindrops, and semi-empirical correlations [20]. However, only the semi-empirical methods allow characterising the exposure of a high number of sites with a reasonable use of time, resources and calculation effort. Thus, ISO 15927-3 and ASHRAE 160P standards describe semi-empirical methods that establish the use of hourly climate data as a starting point for calculating directional WDR exposure [32-33]. This directional calculation is based on the same "WDR relationship" used for the scalar calculation, also incorporating a cosine projection factor *cos (D-θ)*, which relates the wind direction and the orientation of the facade analysed (Eq. 1).

$$WDR_{\theta} = \alpha \cdot U \cdot R_h \cdot \cos\left(D - \theta\right) \tag{1}$$

In this way, the value of WDR_{θ} (l/m^2) over a particular facade orientation θ (º) can be calculated from simultaneous wind velocity records U (m/s), the precipitation intensity R_h (l/m^2) and the wind direction D (º). The result is adjusted using the empirical coefficient α (s/m), which varies according to the particular conditions of each precipitation event. This semi-empirical calculation can also incorporate additional coefficients (wall indices) to reflect the influence of the topography, surroundings, obstructions and geometry of the building on the actual amount of water impinging on each facade.

The ISO 15927-3 standard also includes an exponential adjustment obtained by experimental correction with hourly weather data collected in the United Kingdom [33]. However, many locations lack the hourly climatic data required by ISO and ASHRAE standards (or the datasets are not sufficiently representative), which prevents generalisation of their use. In turn, both the value α and the wall indices introduce a high uncertainty in the calculation: the value α can vary between 0.1 and 0.5 s/m, depending on the precipitation conditions at each moment [20, 34]; the wall indices depend on multiple factors, which, approximately tabulated in the standards, can significantly modulate the result for each specific situation [32-33].

Given these uncertainties, it is customary to simplify Eq. 1 to obtain "airfield" exposure values that obviate the coefficient α and the wall indices (i.e., simplified exposure indices referred to free-standing surroundings with no obstructions for the wind flow). The directional driving-rain index $aDRI_\theta$ (m^2/s) thus represents the exposure on an unobstructed imaginary vertical plane of orientation θ (Eq. 2) calculated from k simultaneous records of R_h (l/m^2), U (m/s) and D (º) collected over the course of N years.

$$aDRI_\theta = \frac{\sum_{i=1}^{k} U_i \cdot \left(\frac{R_{h\,i}}{1000}\right) \cdot \cos\left(D_i - \theta\right)}{N} \qquad (2)$$

The cosine projection factor can also be incorporated into the Bernoulli equation, thus calculating the directional airfield indices referring to wind pressure simultaneous to precipitation. Considering the pressure coefficient C_p equal to 1 and an air density ρ_{air} equal to 1.2 kg/m^3, the directional value of $DRWP_\theta$ (Pa) can be approximated from the m simultaneous records of velocity U (m/s) and wind direction D (º) concurrent with precipitation events during the analysed period (Eq. 3).

$$DRWP_\theta = \frac{\sum_{i=1}^{m} C_p \cdot \frac{1}{2} \cdot \rho_{air} \cdot U_i^{2} \cdot \cos\left(D_i - \theta\right)}{m} \qquad (3)$$

In the summaries included in both Eqs. 2 and 3, only the products of positive value (i.e., those records in which the direction of the wind D causes a positive exposure value on the facade orientation θ) are considered. Thus, it is necessary to perform an independent analysis for each possible facade orientation, discarding those data intervals in which leeward exposure is generated (Fig. 1).

Fig. 1. Directional scheme for the semi-empirical calculation of WDR and DRWP exposures by means of the cosine projection factor cos(D-θ).

The use of this *cos(D-θ)* factor, however, cannot be extrapolated to the more complex and exhaustive CFD calculation methods. Its direct application on the catch ratio that defines these methods (i.e., a parameter of the simulation that represents, through a complicated function of space and time, the interactions between wind velocity, wall indices and coefficient α) results in significant errors in the directional characterisation of WDR exposure [35-36].

In any case, the accuracy of both the CFD methods and the airfield indices presented in Eqs. 2 and 3 is indeed influenced by the time resolution of the climate data used in them [37-38]. The shorter the recording interval duration is, the more accurate the simultaneous wind and rain characterisation is. This reduces the error committed by considering the simultaneity between wind and precipitation, and by averaging the raw measurement data collected in the meteorological stations (co-occurrence and averaging errors, respectively). In this sense, 10-min records are considered exhaustive enough to accurately calculate both exposures, and this is why they are set as reference values when comparing the accuracy of different climate datasets [37, 39-41].

In Part I of this study, the influence of the time resolution of climate datasets on the aDRI and DRWP scalar indices has been analysed, thereby identifying the need to use at least daily records to characterise the wind-driven rain and hourly datasets for the driving-rain wind pressure [13]. The incorporation of a new climate parameter (the wind direction) now causes an additional indetermination, which also varies according to the recording interval used.

To assess this influence, this study analyses two errors that are relevant for the directional characterisation: a quantitative error (e_q), which is associated with the accuracy of the exposure value identified in each possible facade orientation, and an orientation error (e_o), which is related to the correct identification of the exposed orientation.

In 2015, a study based on semi-empirical methods and conducted in 3 Canadian cities concluded that the use of hourly data underestimated the directional value of WDR exposure, compared to that calculated from 5-min records (e_q of 17% for Vancouver, 3.5% for Fredericton, and 14% for Montreal). In addition, the hourly data obtained through the 5-min data arithmetic averaging presented results of greater accuracy than those obtained by other averaging methods (i.e., weighted). In any case, these arithmetic hourly data allowed identifying the most exposed facade orientation, with an e_o value lower than 15º [21].

To the best of the authors' knowledge, the influence of the recording interval on the airfield directional indices obtained by semi-empirical methods has not been systematically characterised (A) by evaluating a significant number of years of records (the aforementioned study only analysed 6-12 months of climatic data), (B) by comparing all the most conventional recording intervals (e.g., including daily and monthly datasets), and (C) by analysing a significant group of sites with different environmental and exposure conditions . In the case of DRWP exposure, these issues have not been addressed in previous studies.

Although raw measurement data are not usually used in semi-empirical calculations (due to their lower availability and higher required calculation effort), real-time recording of climate data in automatic weather stations makes it possible to systematically analyse the uncertainties associated with each possible recording interval.

For this, this study gathers 10-min records obtained during 15 years from 6 automatic stations distributed through the northwest of Spain, developing hourly, daily, monthly and annual datasets by arithmetic averaging. The directional values of $aDRI_\theta$ and $DRWP_\theta$ calculated from these datasets are compared with those based on 10-min data, quantifying the characteristic e_q and e_o errors associated with each recording interval. These results can be used to reduce the uncertainty of directional studies performed using low-time-resolution data, to identify the minimum recording interval required for semi-empirical calculations and to optimise the relationship between error reduction and calculation effort.

Given that the directional airfield index defined in Eq. 2 provides the basis for assessing WDR exposure on specific facades, assessing and reducing these uncertainties complements efforts already made to define more exhaustive wall indices that are close to the accuracy of CFD methods [42-45]. In relation to the DRWP exposure indicators, the study constitutes an initial approach to the analysis of these aspects.

Finally, the relationship between the maximum directional exposure obtained at each location and the scalar exposure value identified at those sites will be examined. The existence of simple linear regressions between both values for the WDR and DRWP exposures has been suggested by a study conducted in 6 Chilean cities from daily datasets [27]. This analysis attempts to verify the existence of these correlations in locations subject to different climatic conditions and for climate datasets with recording intervals that are different from the daily intervals. The confirmation of these adjustments would allow assigning homogeneous designs for all building facades by using the maximum predicted directional value, starting from simple scalar calculations.

3. Directional characterisation of WDR and DRWP airfield indices in Northwestern Spain

The climate records used have been gathered in 6 weather stations in the northwest of Spain (Galicia region): CIS Ferrol, Pedro Murias, Corrubedo, Campus Lugo, Queimadelos and O Invernadeiro. These R_h (l/m^2) and U (m/s) values are the same as those used in the previous scalar analysis (see Part I of this study) but incorporate simultaneous 10-min records of wind direction D (º) for the analysis of directional exposures [13].

The wind direction in each 10-min interval is obtained from raw measurement data with approximation errors <3º, registered by wind vanes equipped with electrical sensors and located at the same height as the anemometer (Fig. 2). All these stations are integrated into the official meteorological network of the Government of Galicia and record the meteorological variables according to the current international standards [13, 46-47]. The fraction of missing data over the analysed period (1 Feb. 2001 – 31 Jan. 2016) ranges from 0.46% to 1.50% (Queimadelos and O Invernadeiro, respectively), which ensures the representativeness of these records.

Datasets corresponding to hourly, daily, monthly and annual intervals were prepared using a spreadsheet program to arithmetically average the more than 780,000 10-min records collected at each station. The wind direction D corresponding to each data interval has been obtained by adding the unit vectors associated with the wind directions recorded along each of them.

Fig. 2. Location of the 6 weather stations and their topography and local considerations in relation to the prevailing winds. *Darker colours represent higher elevations*.

3.1 Prevailing winds during precipitation events in the zone of study

The climate of northwestern Spain is affected by the complex interaction between the North Atlantic Anticyclone (almost permanently located between latitudes 30ºN and 45ºN), the polar front (between latitudes 45ºN and 60ºN) and the characteristic circulations of wind from the west in the Ferrel cell [48-49]. The northern position of the anticyclone during the summer reduces the action of the polar front and the mid-latitude cyclones on the studied region. The clockwise anticyclone circulation causes northwest prevailing winds, alternating precipitation events when the anticyclone oscillates towards the south. In winter, the location of the anticyclone at approximately 30°N allows the area to be influenced by low-pressure areas characterised by southwest prevailing winds and intense rainfall.

Topography is another aspect that also influences the climate configuration of the region. The mountainous north coast is characterised by humid onshore breezes, which are responsible for precipitation distributed throughout the year. On the west and northwest coasts, the numerous ocean-drowned river valleys locally condition the direction of the prevailing winds. Towards the interior, mountain ranges reduce the influence of oceanic winds, channelling it locally according to the orientation of the existing valleys (as for O Invernadeiro or Campus Lugo).

All these considerations are consistent with the characteristic wind roses of the sites studied (Fig. 3). For its elaboration, the generic wind rose (obtained from all the 10-min records of wind direction collected between 2001 and 2016) has been differentiated from the one elaborated using only those records simultaneous to precipitation events. In parallel, the frequency distribution of wind velocities has also been analysed in both cases.

Fig. 3. Prevailing wind directions and velocities considering all available records and only those simultaneous to rainfall events: a) CIS Ferrol; b) Pedro Murias; c) Corrubedo; d) Campus Lugo; e) Queimadelos and f) O Invernadeiro.

As can be observed, the wind presents higher velocities during rainfall intervals, especially at the coastal stations (CIS Ferrol, Pedro Murias and Corrubedo) and those located at higher elevations (O Invernadeiro). In the first two, the most frequent wind velocity during rainfall exceeds 5 m/s, whereas the most common wind velocity during the year is less than 2 m/s. Corrubedo is characterised by its particularly strong winds (predominantly velocities above 5 m/s), whereas the inland wind velocities are drastically reduced (Campus Lugo and Queimadelos).

Wind direction also varies during precipitation events, which prevents the generic wind roses from being used to characterise the WDR and DRWP directional exposures. The O Invernadeiro station (located in the mountainous area of the homonymous natural park) and Campus Lugo (in the valley formed by the

Miño River) are exceptions because the wind direction is strongly restricted by the topographic configuration of its surroundings (W-E and N-SE, respectively). In the remaining stations, the predominance of precipitation from the south and southwest directions is associated with sea-breeze fronts and low-pressure areas.

3.2 Calculations and results

Using Eqs. 2 and 3, the directional exposure indices related to the wind-driven rain and simultaneous wind pressure at each location have been determined. For its calculation, 24 possible facade orientations (i.e., 15 ° intervals) and climate datasets of different time resolutions elaborated from the arithmetic average of the original 10-min records have been considered. For clarity, each exposure index incorporates a prefix *j*, which represents the time resolution of the dataset (i.e., "10" for 10-min, "h" for hourly, "d" for daily, "m" for monthly and "a" for annual datasets). These exposure results are shown in Figs. 4 and 5 (angles are measured in degrees North).

Fig. 4. Directional aDRI values (m^2/s) for different recording intervals: a) CIS Ferrol; b) Pedro Murias; c) Corrubedo; d) Campus Lugo; e) Queimadelos and f) O Invernadeiro.

Fig. 5. Directional DRWP values (Pa) for different recording intervals: a) CIS Ferrol; b) Pedro Murias; c) Corrubedo; d) Campus Lugo; e) Queimadelos and f) O Invernadeiro.

By analysing the 10-min reference results, one can see how the directional distribution of the exposures is consistent with the frequency distribution of wind directions during precipitation events. Most of the sites (CIS Ferrol, Pedro Murias and Queimadelos) exhibit high exposures on southwest-facing facades ranging from 225 to 255º for WDR exposure and from 210 to 225º for DRWP exposure. Corrubedo and Campus

Lugo are subject to greater exposure on the southern facades (180º to 195º), in line with their frequency distribution (Fig. 3). In turn, O Invernadeiro concentrates its exposure on the west-east axis defined by the surrounding topography, with maximum values at 270º N. Significant exposure variations between facades are observed at all sites, with those between 0° and 105° being less exposed to water penetration.

Due to its coastal location, which is subject to strong ocean winds, the maximum directional values of WDR and DRWP are identified in Corrubedo (5.78 m^2/s and 40.01 Pa, respectively). The Campus Lugo station, located in an inland urban environment, represents the most protected location among those analysed (1.02 m^2/s and 3.26 Pa). In general, all coastal sites have higher DRWP exposure, whereas those closest to the west coast are subject to higher WDR.

Figs. 4 and 5 show the influence that the recording interval has on the accuracy of the directional characterisation. It can also be observed how this influence is different for both exposures (WDR and DRWP) and according to the type of error considered (e_q and e_o). Characterising these errors is therefore a key factor for determining the recording interval needed to obtain reliable directional results and for assessing the uncertainty associated with the use of low-time-resolution climate datasets.

4. Error assessment and discussion

To determine the characteristic magnitude of the e_o error associated with each time resolution, the maximum exposure orientations identified by each recording interval (θ_{max}) and that obtained from the 10-min climate dataset were compared. This comparison, even for a single directional exposure value (the one of greatest interest because it has the highest value), serves as a qualitative indicator of the ability of the dataset to determine the exposure in the correct orientation. Table 1 compiles these differences (an uncertainty of ± 15° linked to the amplitude of the 24 intervals defined for the directional analysis must be considered).

Table 1.
Maximum exposure values and its orientation for wind-driven rain (m^2/s) and simultaneous wind pressure (Pa). The orientation error e_o for climate datasets with different time resolutions is also shown.

In the case of WDR exposure, the e_o error is maintained below 45 ° when using hourly and daily datasets. Monthly or annual records present greater uncertainties, with variations that can even surpass 150º (Corrubedo and Campus Lugo). Similar conclusions can be obtained when analysing the DRWP exposure, although the θ_{max} determination exhibits greater accuracy: both hourly and daily records determine this orientation with uncertainties less than 15º. In general, the determination of the most exposed orientation is more inaccurate with a longer dataset recording internal, which makes it advisable to discard data with a time resolution longer than one day. O Invernadeiro constitutes an exception because the greater confinement of the wind directions around the station allows the most exposed orientation to be correctly determined, even when using annual datasets.

Table 1 also compiles the maximum directional exposure values identified using each of the datasets with a different time resolution. In contrast with the scalar values of WDR exposure (see Part I of this research), less-exhaustive recording intervals can overestimate the actual value of the directional exposure. This randomness does not occur in the case of DRWP exposure, where there is a clear tendency to underestimate the maximum exposure, which is more marked in climate data with a poor time resolution.

To characterise the quantitative error associated with the directional exposure value (e_q), the results obtained from each recording interval have again been compared, orientation-by-orientation. The percentage error e_q (%) is calculated by taking the values relative to the 10-min series (Eqs. 4 and 5) as a reference. Thus, Figs. 6 and 7 represent this quantitative error for each of the 24 θ orientations analysed and for each of the sites studied.

$$ {}_{\mathrm{j}}aDRI_{\theta}\ error\ \left(e_q\right) = \frac{100\cdot\left({}_{\mathrm{j}}aDRI_{\theta} - 10'aDRI_{\theta}\right)}{10'aDRI_{\theta}} \tag{4} $$

$$ {}_{\mathrm{j}}DRWP_{\theta}\ error\ \left(e_q\right) = \frac{100\cdot\left({}_{\mathrm{j}}DRWP_{\theta} - 10'DRWP_{\theta}\right)}{10'DRWP_{\theta}} \tag{5} $$

Fig. 6. Percentage error e_q on the directional aDRI values for climate datasets of different time resolution (regarding 10-min values): a) CIS Ferrol; b) Pedro Murias; c) Corrubedo; d) Campus Lugo; e) Queimadelos and f) O Invernadeiro.

Fig. 7. Percentage error e_q on the directional DRWP values for climate datasets of different time resolution (regarding 10-min values): a) CIS Ferrol; b) Pedro Murias; c) Corrubedo; d) Campus Lugo; e) Queimadelos and f) O Invernadeiro.

Although there are important differences between the possible orientations of the same location, the e_q value is greater when the recording interval is longer. Thus, only hourly datasets reflect the directional distribution of the WDR and DRWP exposures with an error of less than 50% in any orientation (relative to the 10-min reference results). The characteristic high exposure of Corrubedo is responsible for the highest e_q values identified at the site. Paradoxically, O Invernadeiro does not have lower errors than other sites despite of its particular topography.

The variability of the e_q errors committed along the D = 24 orientations analysed (even for the hourly datasets) implies that analysing results referring to a single orientation only provides a partial view of the recording interval accuracy. Consequently, to quantify in a general manner the deviations caused by each time resolution, the 24 absolute values of e_q corresponding to each facade orientation (Eqs. 6 and 7) have been averaged. These average results $|e_q|$, together with the values of maximum and minimum oscillation, are compiled in Table 2.

$$ {}_{\mathrm{j}}aDRI\ error\left|e_q\right| = \frac{\sum_{D=1}^{24}\left|{}_{\mathrm{j}}aDRI_{\theta}\ error\ \left(e_q\right)\right|}{24} \quad (6) $$

$$ {}_{\mathrm{j}}aDRI\ error\left|e_q\right| = \frac{\sum_{D=1}^{24}\left|{}_{\mathrm{j}}aDRI_{\theta}\ error\ \left(e_q\right)\right|}{24} \quad (7) $$

Table 2.
Maximum and minimum quantitative error e_q (%) associated with the possible facade orientations and its mean absolute value for each recording interval.

In spite of the different characteristics of the sites studied, the analysis of these $|e_q|$ values shows that there is a similar reliability between directional results obtained from the same time resolution of the dataset. By averaging the $|e_q|$ values of all sites studied, a general guideline for the quantitative uncertainty associated with each recording interval can be obtained (Fig. 8).

Fig. 8. Evolution of mean error $|e_q|$ in aDRI and DRWP directional values for the usual recording intervals used in climate datasets (logarithmic scale).

By taking the 10-min results as a reference, it can be observed how the hourly datasets introduce a mean quantitative error of 7.62% in the $aDRI_\theta$ results. However, this error varies between the stations analysed (depending on their characteristic climatic conditions), presenting a standard deviation σ of 4.7%. This mean error is slightly lower than previously identified at Canadian sites, which were also calculated using arithmetically averaged hourly datasets [21]. These results confirm that the hourly interval (established for the semi-empirical calculation of the WDR exposure by the ISO and ASHRAE standards) can also incorporate relevant errors. Thus, this uncertainty should be considered when the site climate differs from that used to set the empirical adjustments included in these standards (e.g., $\alpha = 2/9$ and exponential adjustment 8/9, for ISO 15927-3). In the case of DRWP exposure, the mean error $|e_q|$ reaches 10.82%, with a σ value of 6.3%. The absence of similar adjustments for the DRWP characterisation implies that in any case, an uncertainty close to 10% in directional results based on hourly data should be assumed.

Considering daily datasets, the mean error amounts to 16.60% for $aDRI_\theta$ values (σ = 3.5%) and 35.70% for DRWP results (σ = 7.8%). The magnitude of these average errors suggests the need to discard daily climate data, at least for the directional calculation of the DRWP exposure. For the same reason, the use of monthly and annual datasets should be excluded, despite its significant reduction in the calculation effort.

In general, the quantitative error associated with the $DRWP_\theta$ indices is similar to that identified in the scalar DRWP values, especially for hourly and daily datasets [13]. However, for the same time resolution, the quantitative error associated with the $aDRI_\theta$ values is greater than that identified for the aDRI scalar values. This difference can be explained by the greater directional error e_o associated with the directional WDR values, which is added to the co-occurrence and averaging errors already present in the scalar calculation. Even so, the $|e_q|$ error is greater in the $DRWP_\theta$ indices than in the $daDRI_\theta$ values, although this difference is reduced and even reversed for the monthly and annual recording intervals.

The representativeness of the climate data and weather stations analysed suggests that these results may be extrapolated to the semi-empirical directional characterisation of other locations with varying environmental conditions. Similarly, these errors should be considered in the comparisons and adjustments established between WDR semi-empirical results and CFD simulations (such as those performed to determine more accurate wall indices), depending on the time resolution of the dataset that was used [42-45].

4.1 Fitting relationships

It follows from the previous section that only the hourly data allows the directional determination of the WDR and DRWP exposures with a quantitative error of less than 15%, also accurately identifying the maximum exposure orientation. However, access to hourly data is not possible in many places, which, together with the high calculation effort required, limits its use and the generalisation of standards such as ISO 15927-3 and ASHRAE 160P. Thus, the attempts to establish more affordable techniques to characterise exposure, starting from climate data with a poor time resolution, are reasonable [20, 24-25].

In this sense, the correlations obtained in Chile between the maximum directional values of the WDR and DRWP exposures, and their respective scalar exposure values, are of particular interest. These adjustments, made from daily datasets collected in 6 sites (Antofagasta, La Serena, Santiago, Concepción, Temuco and Puerto Montt), would allow estimating the most relevant directional value using simple scalar calculations [27]. Because in practice, all building facades are usually designed in a homogeneous manner (regardless of their orientation), it would be possible to establish its required watertightness conditions from this directional maximum extrapolated from scalar exposure values.

By correlating the maximum values of dRI_θ and $dDRWP_\theta$ obtained at each site (Table 1) with their scalar equivalents (see Part I of this study), Fig. 9 identifies the existing correlations and compares them with those obtained in Chile. It is observed that both linear regressions have high coefficients of determination R^2, especially for the DRWP exposure (0.9976). In the case of the WDR exposure, only the data from Queimadelos reduce the accuracy of the adjustment, despite the varied characteristics and exposure conditions of the different analysed locations.

The reasonable convergence of these correlations in two such distant zones (Chile and Spain) confirms the possibility of using this type of regression as a functional alternative to the laborious directional calculation (which must also be repeated for each possible orientation θ analysed). Thus, it is possible to estimate the maximum exposure on the building facades based on a simple scalar calculation (i.e., even in the absence of wind direction records).

It any case and despite the distance between the two zones, the sites also share some common characteristics, such as the climatic influence exerted by nearby oceans and their location at similar latitudes (in different hemispheres). Therefore, the analysis of a greater number of sites and the characterisation of other geographical areas remain a necessary task to improve these regressions and refine the scope of their validity.

Fig. 9. Best-fit linear relationships between the scalar and maximum directional values for the WDR and DRWP exposures. Comparison with the correlations identified in Chile (dashed line).

To more accurately estimate the maximum directional exposure, Table 3 compiles and relates the scalar exposure values associated with each recording interval, with the maximum values $10'aDRI_{\theta}$ and $10'DRWP_{\theta}$. For the DRWP exposure, all best fit-linear relationships have a coefficient of determination greater than 0.8, which ensures a reasonable estimation of the maximum $10'DRWP_{\theta}$ value even using scalar indices of low-time resolution. On the other hand, only the scalar indices 10'aDRI and haDRI allow estimating the maximum $10'aDRI_{\theta}$ value with an R^2 greater than 0.8.

Table 3.
Maximum directional values of 10’aDRI (m^2/s) and 10’DRWP (Pa) and their correlation with the scalar exposure values [13].

5. Conclusions

This work has clarified the influence that the choice or availability of a particular recording interval dataset has on the accuracy of the semi-empirical directional indices that characterise the WDR and

DRWP exposures. By analysing exhaustive climatic data gathered in automatic weather stations and other datasets of conventional time resolutions, guidelines have been obtained to contextualise the results of the WDR and DRWP calculations. The representativeness of the analysed data and stations supports the possibility of extrapolating these guidelines to a wide variety of situations and exposure conditions.

The study demonstrates that only the hourly climate data accurately determine the directional values of $aDRI_{\theta}$ and $DRWP_{\theta}$, in addition to correctly identifying the maximum exposure. Even so, hourly records can generate non-negligible errors (close to 10%) in both indices. Less-exhaustive datasets such as monthly or annual data should be discarded, given the significant uncertainties their directional outcomes.

In turn, the existence of precise correlations between the maximum directional exposure value and the scalar exposure value has been confirmed. Using datasets with low time resolution or lacking wind direction records, these adjustments allow estimating the maximum directional exposure received at the site. The construction codes could use these maximum values, obtained through these functional correlations, to establish general watertightness conditions for any facade of the building, thus maintaining the homogeneous design typical of construction enclosures.

Together, the results obtained in both parts of this study allow reducing the uncertainty of the semi-empirical calculations (scalar and directional), identifying the minimum recording interval required to determine these exposures and optimising the relationship between the error reduction and the calculation effort. Given that the airfield indices analysed constitute the starting point for obtaining actual exposures on specific facades (e.g., by applying the appropriate wall indices), these improvements should contribute to the refinement of future designs under various exposure conditions.

Acknowledgements

This work was partially financed by the Spanish Ministry of Science and Innovation and the FICYT co-financed with FEDER funds under the Research Projects BIA2012-31609 and FC-15-GRUPIN14-004.

References

[1] Lacasse MA, O'Connor T, Nunes SC, Beaulieu P. (2003). Report from Task 6 of MEWS Project: Experimental assessment of water penetration and entry into wood-frame wall specimens – Final Report (Institute for Research in Construction - Internal Report 113). Ottawa: National Research Council Canada; 2003.

[2] Cornick SM, Lacasse MA. A review of climate loads relevant to assessing the watertightness performance of walls, windows, and wall-window interfaces. *J ASTM Int 2005;* 2(10):1-16. http://dx.doi.org/10.1520/JAI12505.

[3] Franke L, Schumann I, van Hees R, van der Klugt L, Naldani S, Binda L, et al. Damage atlas: classification and analyses of damage patterns found in brick masonry (Protection and Conservation of European Cultural Heritage, Research Report Nr 8, vol 2). Stuttgart: Fraunhofer IRB Verlag; 1998.

[4] Kvande T, Lisø KR. Climate adapted design of masonry structures. *Build Environ 2009;* 44:2442-50. http://dx.doi.org/10.1016/j.buildenv.2009.04.007.

[5] Ruedrich J, Bartelsen T, Dohrmann R, Siesgemund S. Moisture expansion as a deterioration factor for sandstone used in buildings. Environ Earth Sci 2011; 63:1545-64. http://dx.doi.org/10.1007/s12665-010-0767-0.

[6] Steiger M, Charola E, Sterflinger K. Weathering and deterioration. In: Siesgesmund S, Snethlage R, editors. Stone in architecture. Berlin: Springer-Verlag Berlin; 2011, p. 227-316.

[7] Jerman M, Černý R. Effect of moisture content on heat and moisture transport and storage properties of thermal insulation materials. Energ Buildings 2012; 53:39-46. http://dx.doi.org/10.1016/j.enbuild.2012.07.002.

[8] Dell'Isola M, d'Ambrosio FR, Giovinco GE, Ianniello E. Experimental analysis of thermal conductivity for building materials depending on moisture content. Int J Thermophys 2013; 33:1674-85. http://dx.doi.org/10.1007/s10765-012-1215-z.

[9] Li FGN, Smith AZP, Biddulph P, Hamilton IG, Lowe R, Mavrogianni A, et al. Solid-wall U-values: heat flux measurements compared with standard assumptions. Build Res Inf 2015; 43:238-52. http://dx.doi.org/10.1080/09613218.2014.967977.

[10] Coelho GBA, Henriques FMA. Influence of driving rain on the hygrothermal behavior of solid brick walls. Journal of Building Engineering 2016; 7:121-32. http://dx.doi.org/10.1016/j.jobe.2016.06.002.

[11] Andersen B, Frisvad JC, Søndergaard I, Rasmussen IS, Larsen LS. Associations between fungal species and water-damaged building materials. Appl Environ Microb 2011; 77:4180-8. http://dx.doi.org/10.1128/AEM.02513-10.

[12] Sauni R, Verbeek JH, Uitti J, Jauhiainen M, Kreiss K, Sigsgaard T. Remediating buildings damaged by dampness and mould for preventing or reducing respiratory tract symptoms, infections and asthma. In, *Cochrane Database of Systematic Reviews* 2:CD007897; 2015. http://dx.doi.org/10.1002/14651858.CD007897.pub3.

[13] Pérez JM, Domínguez J, Cano E, del Coz JJ. On the significance of climate-dataset recording interval in characterising wind-driven rain and simultaneous wind pressure. Part I: Scalar approach. (Under review; Previous and complementary part of this study).

[14] Sahal N, Lacasse MA. Proposed method for calculating water penetration test parameters of wall assemblies as applied to Istanbul, Turkey. Build Environ 2008; 43:1250–60. http://dx.doi.org/10.1016/j.buildenv.2007.03.009.

[15] Pérez JM, Domínguez J, Rodríguez B, del Coz JJ, Cano E. A new method for determining the water tightness of building facades. Build Res Inf 2013; 41(4):401-14. http://dx.doi.org/10.1080/09613218.2013.774936.

[16] Van den Bossche N, Lacasse MA, Janssens A. A uniform methodology to establish test parameters for watertightness testing. Part I: A critical review. Build Environ 2013; 63:145-56. http://dx.doi.org/10.1016/j.buildenv.2012.12.003.

[17] Van den Bossche N, Lacasse MA, Janssens A. A uniform methodology to establish test parameters for watertightness testing. Part II: Pareto front analysis on co-occurring rain and wind. Build Environ 2013; 63:157-67. http://dx.doi.org/10.1016/j.buildenv.2012.12.019.

[18] Pérez JM, Domínguez J, Cano E, del Coz JJ, Suárez FJ. A comparison of methods for determining watertightness test parameters of building façades. Build Environ 2014; 78:145-54. http://dx.doi.org/10.1016/j.buildenv.2014.04.027.

[19] Prior MJ. Directional driving rain indices for the United Kingdom. Computation and mapping. Building Research Establishment Report, Garston: Department of the Environment, Building Research Establishment, Building Research Station; 1985.

[20] Blocken B, Carmeliet, J. A review of wind-driven rain research in building science. J Wind Eng Ind Aerodyn 2004; 92(13):1079-130. http://dx.doi.org/10.1016/j.jweia.2004.06.003.

[21] Ge H. Influence of time resolution and averaging techniques of meteorological data on the estimation of wind-driven rain load on building facades for Canadian climates. J Wind Eng Ind Aerodyn 2015; 143:50-61. http://dx.doi.org/10.1016/j.jweia.2015.04.019.

[22] Zhu D, Mallidi SR, Fazio P. Approach for urban driving rain index by using climatological data recorded at suburban meteorological station. Build Environ 1995; 30(2): 229-36. http://dx.doi.org/10.1016/0360-1323(94)00049-X.

[23] Underwood JS, Meentemeyer V. Climatology of wind-driven rain for the contiguous United States for the period 1971 to 1995. Phys Geogr 1998; 19(6):445-62. http://dx.doi.org/10.1080/02723646.1998.10642661.

[24] Rydock JP, Lisø KR, Førland EJ, Nore K, Thue JV. A driving rain exposure index for Norway. Build Environ 2005; 40:1450-8. http://dx.doi.org/10.1016/j.buildenv.2004.11.018.

[25] Rydock JP, Gustavsen A. A look at driving rain spells at three cities in Great Britain. Build Environ 2007; 42:1386-90. http://dx.doi.org/10.1016/j.buildenv.2005.11.020.

[26] Ge H, Krpan R. Wind-driven Rain Study in the Coastal Climate of British Columbia. Final Report. Burnaby, British Columbia: British Columbia Institute of Technology; 2009.

[27] Pérez JM, Domínguez J, Cano E, del Coz JJ, Alonso M. Global analysis of building façade exposure to water penetration in Chile. Build Environ 2013; 70:284-297. http://dx.doi.org/10.1016/j.buildenv.2013.09.001.

[28] Basist A, Bell GD. Statistical relationships between topography and precipitation patterns. J Climate 1994; 7(9):1305-15. http://dx.doi.org/10.1175/1520-0442(1994)007<1305:SRBTAP>2.0.CO;2

[29] Chen CS, Chen YL. The rainfall characteristics of Taiwan. Mon Wea Rev 2003; 131(7):1323-41. http://dx.doi.org/10.1175/1520-0493(2003)131<1323:TRCOT>2.0.CO;2

[30] Roe GH. Orographic precipitation. Annu Rev Earth Planet Sci 2005; 33:645-71. http://dx.doi.org/10.1146/annurev.earth.33.092203.122541.

[31] Hand LM, Shepherd JM, An investigation on warm-season spatian rainfall variability in Oklahoma city: Possible linkages to urbanización and prevailing wind. J Appl Meteor Climatol 2009; 48(2):251-69. http://dx.doi.org/10.1175/2008JAMC2036.1.

[32] ANSI/ASHRAE Standard 160. Criteria for moisture-control design analysis in buildings. American Society of Heating and Air-Conditioning Engineers, Atlanta; 2009.

[33] EN ISO 15927-3. Hygrothermal performance of buildings. Calculation and presentation of climatic data. Part 3: calculation of a driving rain index for vertical surfaces from hourly wind and rain data. European Committee for Standardization; 2009.

[34] Straube JF, Burnett EFP. Simplified prediction of driving rain deposition. In: Proceedings of International Building Physics Conference. Eindhoven; 2000, p. 375-82.

[35] Blocken B, Carmeliet J. On the validity of the cosine projection in wind-driven rain calculations on buildings. Building and Environment 2006; 41(9):1182-9. http://dx.doi.org/10.1016/j.buildenv.2005.05.002.

[36] Blocken B, Carmeliet J. Validation on CFD simulations of wind-driven rain on a low-rise building façade. Build Environ 2007; 42(7):2530-48. http://dx.doi.org/:10.1016/j.buildenv.2006.07.032

[37] Blocken B, Carmeliet J. On the errors associated with the use of hourly data in wind-driven rain calculations on building facades. Atmos Environ 2007; 41:2335-43. http://dx.doi.org/10.1016/j.atmosenv.2006.11.014.

[38] Blocken B, Carmeliet J. Guidelines for the required time resolution of meteorological input data for wind-driven rain calculations on buildings. J Wind Eng Ind Aerodyn 2008; 96:621-39. http://dx.doi.org/10.1016/j.jweia.2008.02.008.

[39] Van der Hoven I. Power spectrum of horizontal wind speed in the frequency range from 0.0007–900 cycles per hour. J Meteorol 1957; 14:160–4. http://dx.doi.org/10.1175/1520-0469(1957)014<0160:PSOHWS>2.0.CO;2.

[40] Jones DMA, Sims AL. Climatology of instantaneous rainfall rates. J Appl Meteorol 1978; 17:1135–50. http://dx.doi.org/10.1175/1520-0450(1978)017<1135:COIRR>2.0.CO;2.

[41] Sumner GN. Precipitation: Process and Analysis. New York: John Wiley and Sons; 1988.

[42] Blocken B, Carmeliet J. 2010. Overview of three state-of-the-art wind-driven rain assessment models and comparison based on model theory. Build Environ 2010; 45(3): 691-703. http://dx.doi.org/10.1016/j.buildenv.2009.08.007

[43] Blocken B, Deszö G, van Beeck J, Carmeliet J. Comparison of calculation models for wind-driven rain deposition on building facades. Atmos Environ 2010; 44:1714-25. http://dx.doi.org/10.1016/j.atmosenv.2010.02.011

[44] Blocken B, Abuku M, Nore K., Briggen PM, Schellen HL, Thue JV, et al. Intercomparison of wind-driven rain deposition models based on two case studies with full-scale measurements. J Wind Eng Ind Aerodyn 2011; 99(4):448-59. http://dx.doi.org/10.1016/j.jweia.2010.11.004

[45] Ge H, Deb Nath UK, Chiu V. Field measurements of wind-driven rain on mid- and high-rise buildings in three Canadian regions. Build Environ 2017; 116:228-245. http://dx.doi.org/10.1016/j.buildenv.2017.02.016

[46] WMO. Guide to Meteorological Instruments and Methods of Observation. WMO-No 8.Geneva: World Meteorological Organization; 2008.

[47] Xunta of Galicia. Department of Environment, Territory and Infrastructures. Galicia, Spain. <http://www.meteogalicia.gal/> [Last accessed 19.05.2017].

[48] Davis RE, Hayden BP, Gay DA, Phillips WL, Jones G. The North Atlantic Subtropical Anticyclone. J Climate 1997; 10(4):728-44. http://dx.doi.org/10.1175/1520-0442(1997)010<0728:TNASA>2.0.CO;2

[49] Lorenzo MN, Taboada JJ, Gimeno L. Links between circulation weather types and teleconnection patterns and their influence on precipitation patterns in Galicia (NW Spain). Int J Climatol 2008; 28(11):1493-505. http://dx.doi.org/10.1002/joc.1646

Highlights

- Study of 10-min, hourly, daily, monthly and annually climatic data, over 15 years
- Directional characteristation of the WDR and DRWP exposures in varied locations
- Influence of dataset time resolution on the accuracy of these directional exposures
- Cuantitative and orientation errors associated with each possible recording interval
- Useful correlations to determine maximum directional exposure from scalar values

List of tables

Table 1

Table 1.
Maximum exposure values and its orientation for wind-driven rain (m^2/s) and simultaneous wind pressure (Pa). Orientation error e_o for climate datasets with different time resolutions is also shown.

	$10'aDRI_\theta$		$haDRI_\theta$			$daDRI_\theta$			$maDRI_\theta$			$aaDRI_\theta$		
	Max.	θ_{max}	Max.	θ_{max}	e_o	Max.	θ_{max}	e_o	Max.	θ_{max}	e_o	Max	θ_{max}	e_o
CIS Ferrol	2.90	240	2.90	225	15º	2.84	210	30º	1.79	255	15º	3.28	330	90º
Pedro Murias	1.93	255	1.94	240	15º	2.01	210	45º	1.83	195	60º	1.84	180	75º
Corrubedo	5.78	195	5.90	180	15º	4.77	195	0º	2.31	165	30º	2.74	45	150º
Campus Lugo	1.02	195	1.00	180	15º	0.99	180	15º	0.82	15	180º	1.23	15	180º
Queimadelos	3.31	225	3.42	225	0º	3.08	225	0º	1.61	210	15º	1.60	225	0º
O Invernadeiro	2.71	270	2.76	255	15º	2.93	270	0º	3.57	270	0º	3.59	270	0º
	$10'DRWP_\theta$		**$hDRWP_\theta$**			**$dDRWP_\theta$**			**$mDRWP_\theta$**			**$aDRWP_\theta$**		
	Max.	θ_{max}	Max.	θ_{max}	e_o	Max.	θ_{max}	e_o	Max.	θ_{max}	e_o	Max	θ_{max}	e_o
CIS Ferrol	9.03	210	8.66	210	0º	7.53	210	0º	4.72	15	165º	4.92	330	120º
Pedro Murias	9.72	210	9.78	210	0º	8.96	210	0º	6.07	210	0º	5.52	180	30º
Corrubedo	40.01	195	35.39	195	0º	21.10	195	0º	9.28	180	15º	11.49	285	90º
Campus Lugo	3.26	180	2.91	180	0º	2.30	165	15º	1.79	0	180º	1.61	0	180º
Queimadelos	3.31	225	2.88	225	0º	1.72	210	15º	0.97	105	120º	1.15	75	150º
O Invernadeiro	7.45	270	6.66	270	0º	4.16	270	0º	3.20	270	0º	3.17	270	0º

Table 2

Table 2.
Maximum and minimum quantitative error e_q (%) associated with the possible facade orientations and its mean absolute value for each recording interval.

	$haDRI_\theta$			**$daDRI_\theta$**			**$maDRI_\theta$**			**$aaDRI_\theta$**		
	$e_{q\ max}$	$e_{q\ min}$	$\lvert e_q\rvert$	$e_{q\ max}$	$e_{q\ min}$	$\lvert e_q\rvert$	$e_{q\ max}$	$e_{q\ min}$	$\lvert e_q\rvert$	$e_{q\ max}$	$e_{q\ min}$	$\lvert e_q\rvert$
CIS Ferrol	-13.4	-0.4	6.3	-25.9	-0.5	10.9	-45.7	-0.6	29.7	+148.6	+9.7	82.6
Pedro Murias	-16.1	-0.2	7.2	+33.6	-1.4	16.4	-85.3	-0.4	39.6	+109.7	+1.9	58.8
Corrubedo	-10.3	-0.1	4.8	+39.1	+1.7	15.1	+171.1	-4.8	62.1	+532.0	+26.5	151.0
Campus Lugo	-15.6	+0.4	7.6	-60.4	-0.7	16.7	-71.9	+7.5	38.9	+114.9	-8.5	72.0
Queimadelos	-44.3	+0.2	16.7	-49.2	-5.6	20.7	+139.1	-0.2	60.4	+119.7	+1.8	54.9
O Invernadeiro	-7.2	-0.2	3.1	-79.8	+2.7	19.8	-96.9	-4.3	61.2	-100.0	+1.1	65.2

	$hDRWP_\theta$			**$dDRWP_\theta$**			**$mDRWP_\theta$**			**$aDRWP_\theta$**		
	$e_{q\ max}$	$e_{q\ min}$	$\lvert e_q\rvert$	$e_{q\ max}$	$e_{q\ min}$	$\lvert e_q\rvert$	$e_{q\ max}$	$e_{q\ min}$	$\lvert e_q\rvert$	$e_{q\ max}$	$e_{q\ min}$	$\lvert e_q\rvert$
CIS Ferrol	-12.8	+0.4	6.8	-56.0	+1.5	27.0	-53.7	-30.7	43.8	-100.0	-19.7	62.1
Pedro Murias	+15.2	+0.2	6.6	-55.5	-7.7	25.1	-78.9	-31.7	47.8	-100.0	-24.9	54.9
Corrubedo	-17.5	-3.3	9.3	-65.5	-6.1	38.7	-78.2	-7.3	58.6	+110.4	-9.6	68.2
Campus Lugo	-16.8	-1.9	11.2	-72.1	-18.5	38.2	-70.8	-24.4	50.9	-88.7	-34.7	55.0
Queimadelos	-44.9	-13.0	23.1	-77.5	-12.1	44.6	-74.3	-4.3	46.1	-81.7	+2.0	50.9
O Invernadeiro	-13.6	-1.7	7.9	-88.1	-18.2	40.6	-79.6	-56.5	66.8	-100.0	-56.4	82.1

Table 3

Table 3.
Maximum directional values of 10’aDRI (m^2/s) and 10’DRWP (Pa) and its correlation with their scalar exposure values [13].

	Max. 10’aDRI$_\theta$	10’aDRI	haDRI	daDRI	maDRI	aaDRI
CIS Ferrol	2.90	5.02	4.86	4.76	4.00	3.97
Pedro Murias	1.93	3.66	3.59	3.59	2.93	2.71
Corrubedo	5.78	7.98	7.99	7.00	4.60	4.07
Campus Lugo	1.02	2.23	2.18	2.06	1.67	1.71
Queimadelos	3.31	4.07	4.05	3.62	2.65	2.50
O Invernadeiro	2.71	5.39	5.36	4.83	3.74	3.61

Max. 10'aDRI$_\theta$ = 0.731 · 10'aDRI – 0.650 ($R^2 = 0.819$)
Max. 10'aDRI$_\theta$ = 0.732 · haDRI – 0.617 ($R^2 = 0.832$)
Max. 10'aDRI$_\theta$ = 0.818 · daDRI – 0.712 ($R^2 = 0.765$)
Max. 10'aDRI$_\theta$ = 0.996 · maDRI – 0.528 ($R^2 = 0.567$)
Max. 10'aDRI$_\theta$ = 0.996 · aaDRI – 0.323 ($R^2 = 0.456$)

	Max. 10’DRWP$_\theta$	10’DRWP	hDRWP	dDRWP	mDRWP	aDRWP
CIS Ferrol	9.03	11.41	10.61	8.29	6.11	5.96
Pedro Murias	9.72	11.10	10.84	8.67	5.51	5.19
Corrubedo	40.01	40.82	35.90	22.04	10.83	10.18
Campus Lugo	3.26	4.20	3.63	2.56	1.99	1.92
Queimadelos	3.31	3.57	3.00	1.84	1.24	1.20
O Invernadeiro	7.45	8.02	7.06	4.56	3.24	3.19

Max. 10'DRWP$_\theta$ = 1.008 · 10'DRWP – 1.158 ($R^2 = 0.996$)
Max. 10'DRWP$_\theta$ = 1.144 · hDRWP – 1.394 ($R^2 = 0.992$)
Max. 10'DRWP$_\theta$ = 1.853 · dDRWP – 2.627 ($R^2 = 0.957$)
Max. 10'DRWP$_\theta$ = 3.749 · mDRWP – 5.813 ($R^2 = 0.855$)
Max. 10'DRWP$_\theta$ = 3.989 · aDRWP – 6.077 ($R^2 = 0.846$)

Figure captions

Fig. 1. Directional scheme for the semi-empirical calculation of WDR and DRWP exposures by means of the cosine projection factor cos(D-θ).

Fig. 2. Location of the 6 weather stations and their topography and local considerations in relation to the prevailing winds. *Darker colours represent higher elevations*.

Fig. 3. Prevailing wind directions and velocities considering all available records and only those simultaneous to rainfall events: a) CIS Ferrol; b) Pedro Murias; c) Corrubedo; d) Campus Lugo; e) Queimadelos and f) O Invernadeiro.

Fig. 4. Directional aDRI values (m^2/s) for different recording intervals: a) CIS Ferrol; b) Pedro Murias; c) Corrubedo; d) Campus Lugo; e) Queimadelos and f) O Invernadeiro.

Fig. 5. Directional DRWP values (Pa) for different recording intervals: a) CIS Ferrol; b) Pedro Murias; c) Corrubedo; d) Campus Lugo; e) Queimadelos and f) O Invernadeiro.

Fig. 6. Percentage error e_q on the directional aDRI values for climate datasets of different time resolution (regarding 10-min values): a) CIS Ferrol; b) Pedro Murias; c) Corrubedo; d) Campus Lugo; e) Queimadelos and f) O Invernadeiro.

Fig. 7. Percentage error e_q on the directional DRWP values for climate datasets of different time resolution (regarding 10-min values): a) CIS Ferrol; b) Pedro Murias; c) Corrubedo; d) Campus Lugo; e) Queimadelos and f) O Invernadeiro.

Fig. 8. Evolution of mean error $|e_q|$ in aDRI and DRWP directional values for the usual recording intervals used for climate datasets (logarithmic scale).

Fig. 9. Best fit-linear relationships between the scalar and maximum directional values for the WDR and DRWP exposures. Comparison with the correlations identified in Chile (dashed line).

Figure 1

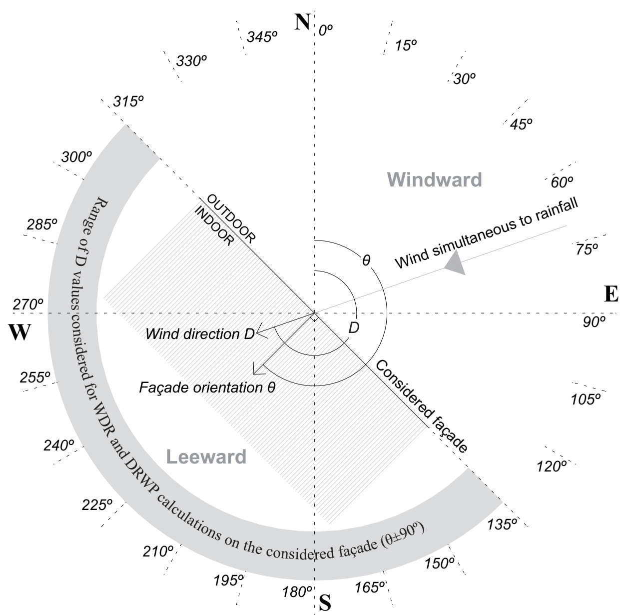

Fig. 1. Directional scheme for the semi-empirical calculation of WDR and DRWP exposures by means of the cosine projection factor cos(D-θ).

Figure 2

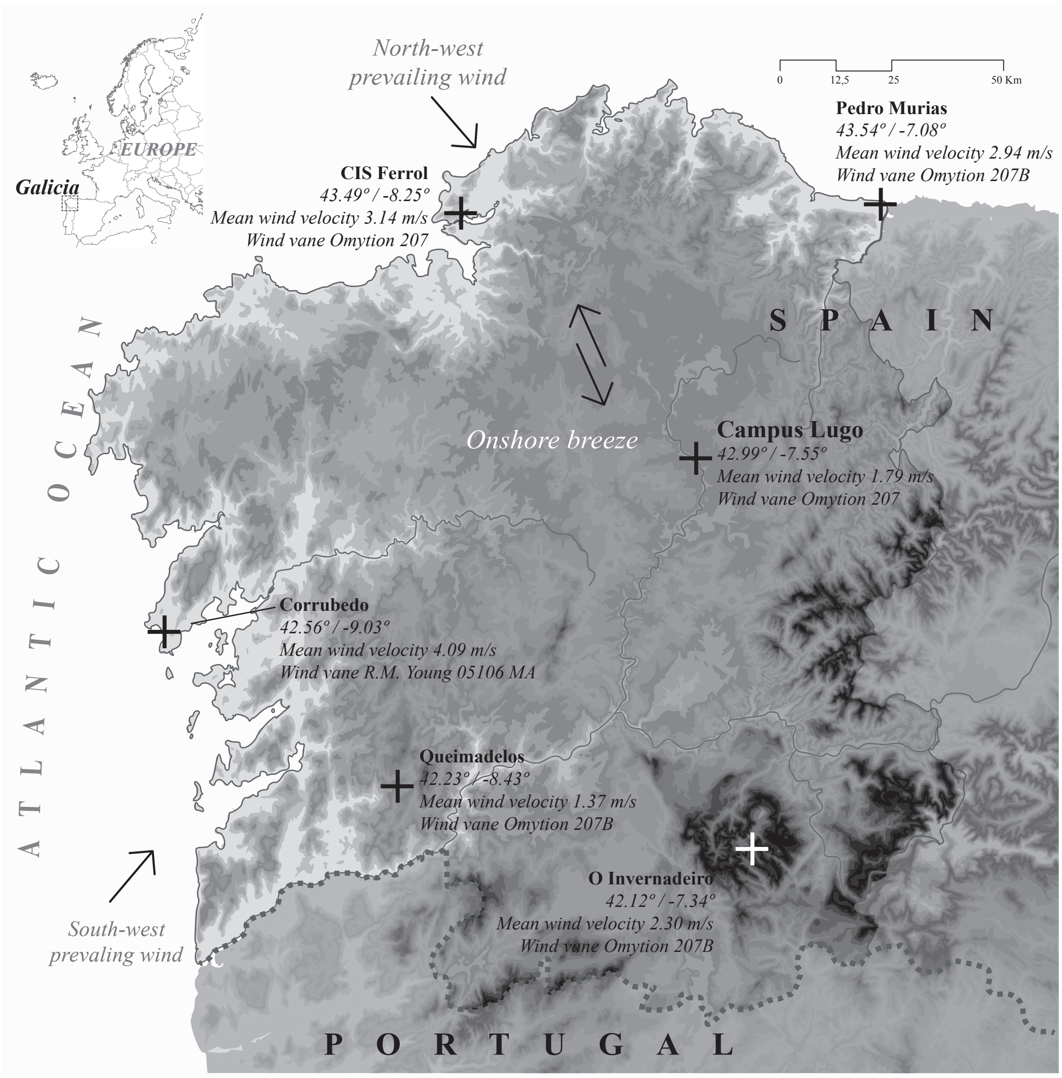

Fig. 2. Location of the 6 weather stations and their topography and local considerations in relation to the prevailing winds. *Darker colours represent higher elevations.*

Figure 3

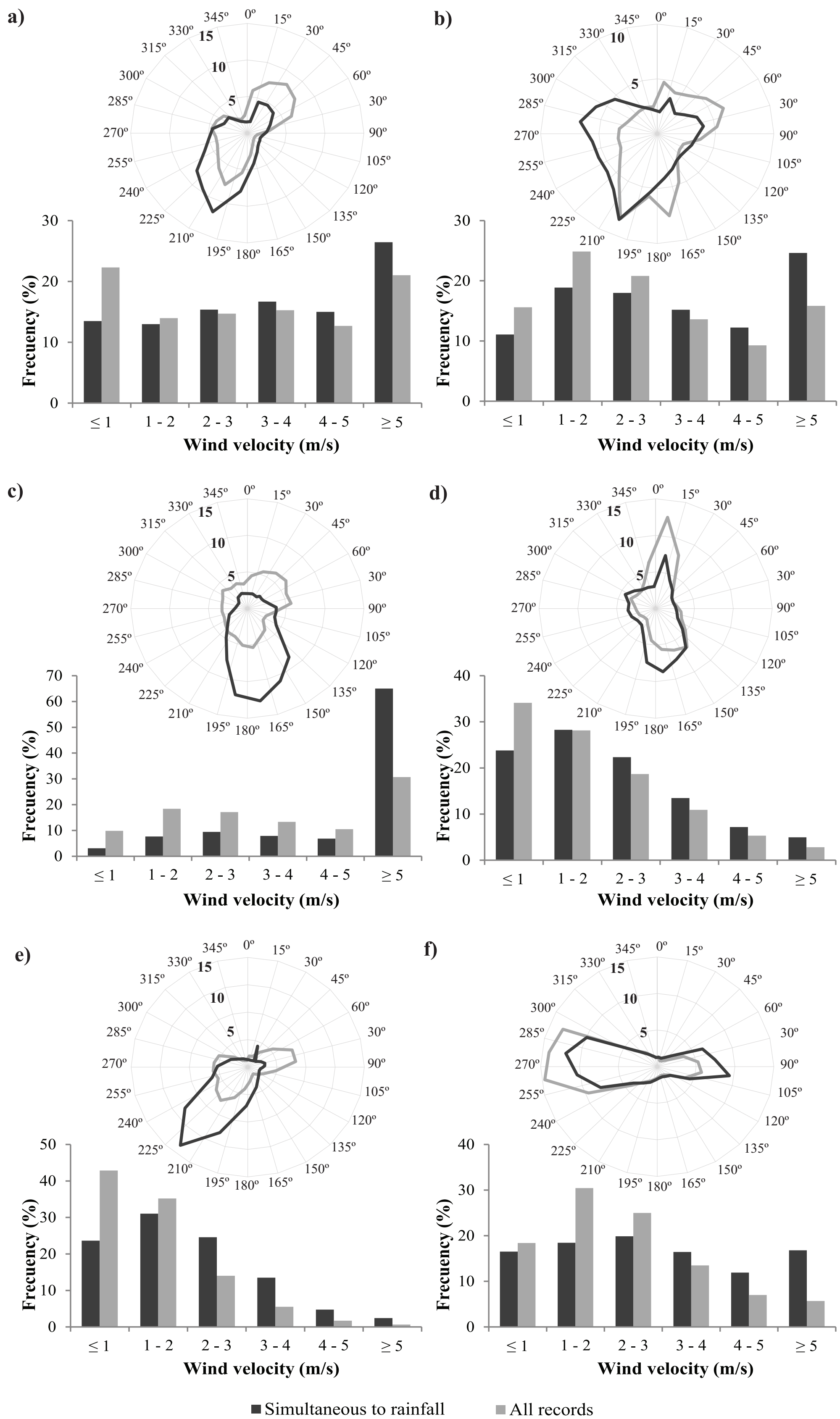

Fig. 3. Prevailing wind directions and velocities considering all available records and only those simultaneous to rainfall events: a) CIS Ferrol; b) Pedro Murias; c) Corrubedo; d) Campus Lugo; e) Queimadelos and f) O Invernadeiro.

Figure 4

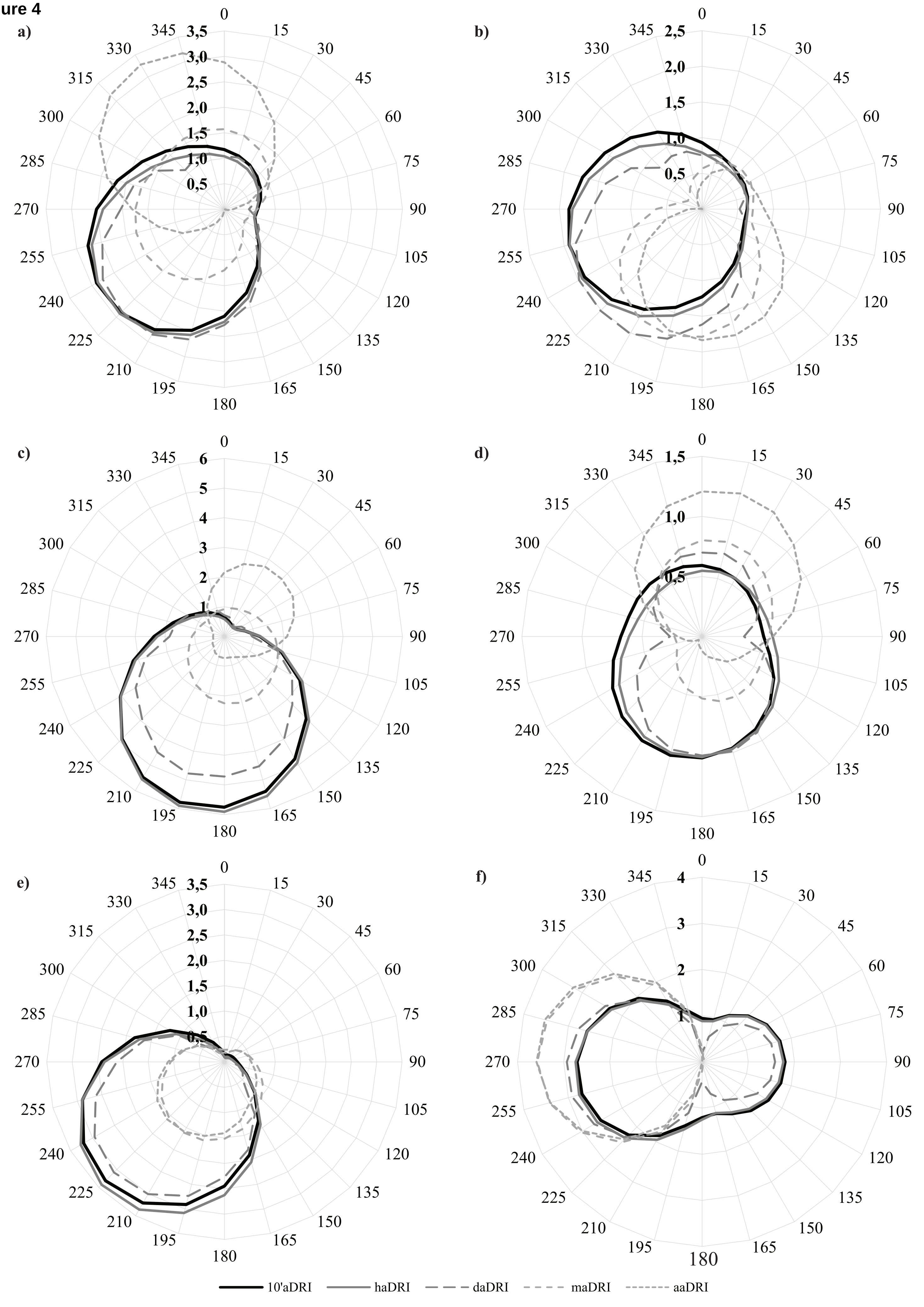

Fig. 4. Directional aDRI values (m^2/s) for different recording intervals:
a) CIS Ferrol; b) Pedro Murias; c) Corrubedo; d) Campus Lugo; e) Queimadelos and f) O Invernadeiro.

Figure 5

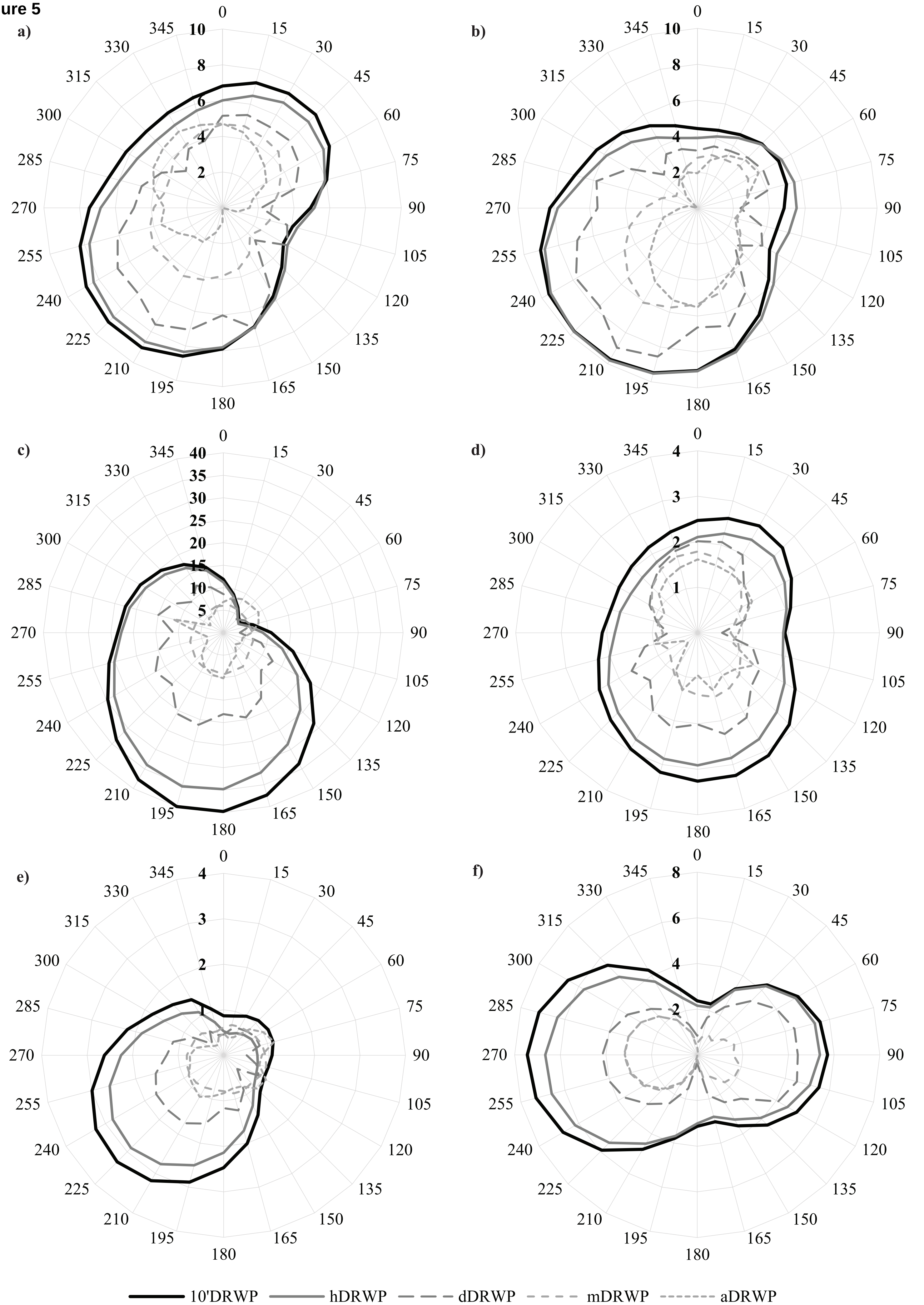

Fig. 5. Directional DRWP values (Pa) for different recording intervals:
a) CIS Ferrol; b) Pedro Murias; c) Corrubedo; d) Campus Lugo; e) Queimadelos and f) O Invernadeiro.

Figure 6

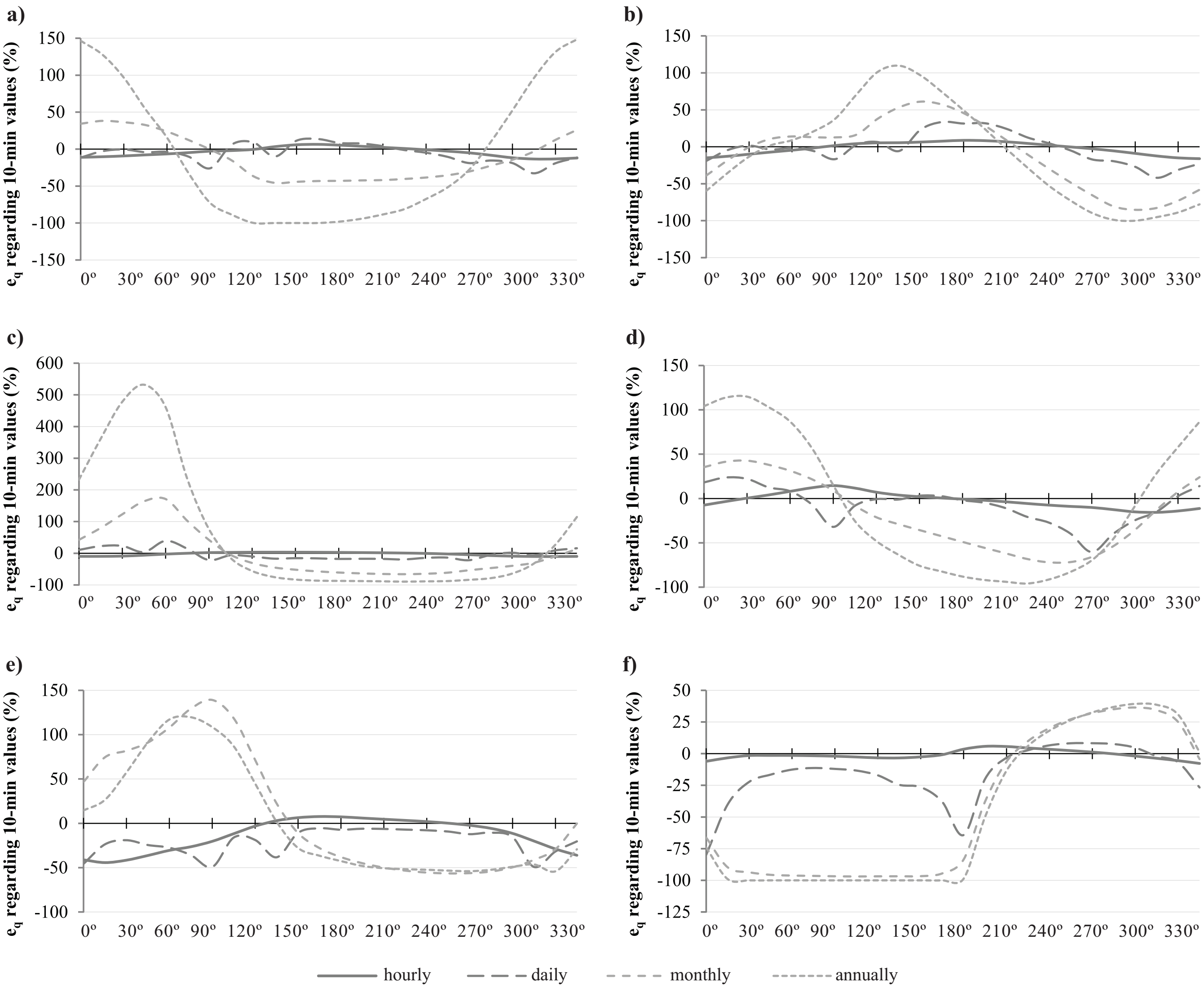

Fig. 6. Percentage error e_q on the directional aDRI values for climate datasets of different time resolution (regarding 10-min values): a) CIS Ferrol; b) Pedro Murias; c) Corrubedo; d) Campus Lugo; e) Queimadelos and f) O Invernadeiro.

Figure 7

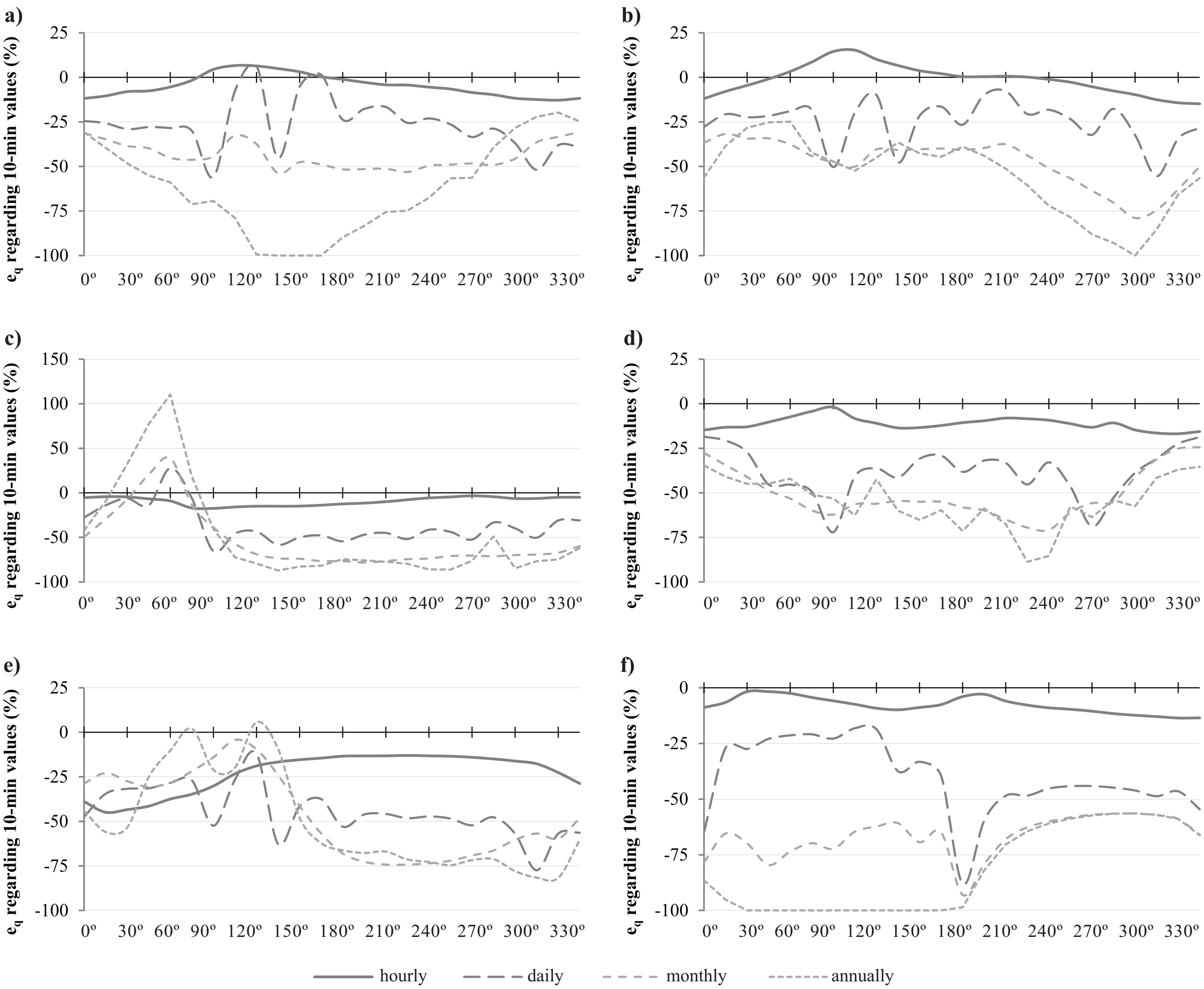

Fig. 7. Percentage error e_q on the directional DRWP values for climate datasets of different time resolution (regarding 10-min values): a) CIS Ferrol; b) Pedro Murias; c) Corrubedo; d) Campus Lugo; e) Queimadelos and f) O Invernadeiro.

Figure 8

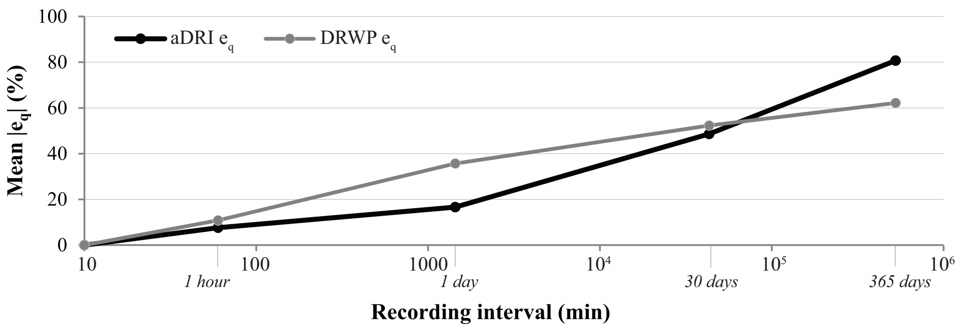

(%)	Hourly dataset	Daily dataset	Monthly dataset	Annual dataset
aDRI mean error $\|e_q\|$	7.62	16.60	48.65	80.75
Standard deviation	*4.7*	*3.5*	*14.2*	*35.8*

(%)	Hourly dataset	Daily dataset	Monthly dataset	Annual dataset
DRWP mean error $\|e_q\|$	10.82	35.70	52.33	62.20
Standard deviation	*6.3*	*7.8*	*8.8*	*11.5*

Fig. 8. Evolution of mean error $|e_q|$ in aDRI and DRWP directional values for the usual recording intervals used for climate datasets (logarithmic scale).

Figure 9

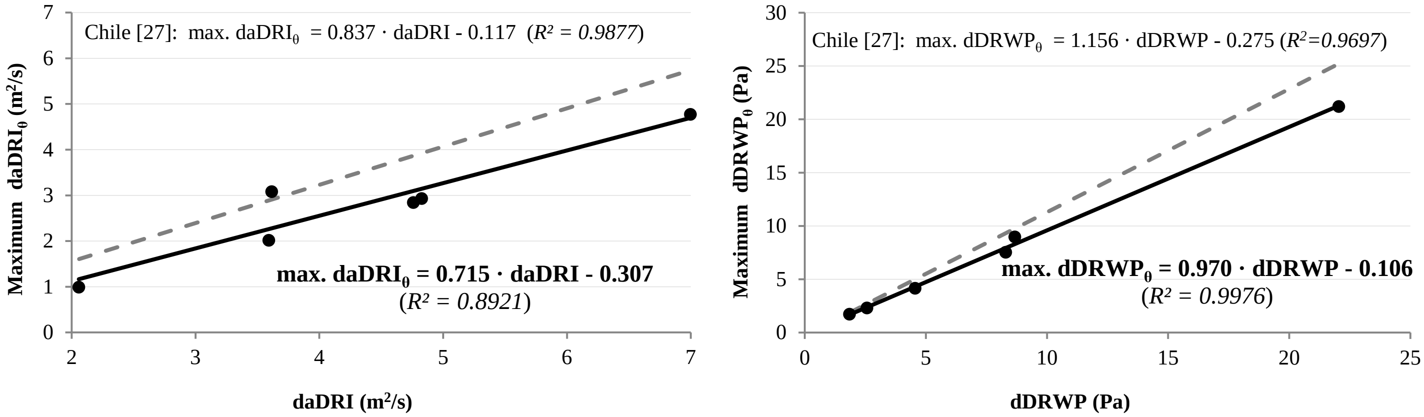

Fig. 9. Best fit-linear relationships between the scalar and maximum directional values for the WDR and DRWP exposures. Comparison with the correlations identified in Chile (dashed line).